Int J Adv Manuf Technol (2016) 84:2707–2718
DOI 10.1007/s00170-015-7839-y

ORIGINAL ARTICLE

# Effects of blank dimension on forming characteristics during conical-section ring rolling of Inco718 alloy

**Xinglin Zhu[1] · Dong Liu[1] · Yanhui Yang[1] · Yang Hu[1] · Guowei Liu[1] · Yuanning Wang[2]**

Received: 8 January 2015 / Accepted: 13 September 2015 / Published online: 7 October 2015


**Abstract** For profile ring rolling of difficult-to-deform materials, geometry and dimensions of blank are critical for dimensional accuracy and thermomechanical parameters distribution of the formed ring. In this study, four blank design principles for conical-section ring rolling are presented based on analytical description of the volume distribution characteristic curve (VDCC), and then effects of all dimension factors of the four blanks are explored comprehensively by using 3D coupled thermomechanical FE model established based on FORGE. According to the comprehensive analysis, optimal blank design principle for conical-section ring rolling is determined. The results obtained show that: (1) Preparation stage of rolling process (PSRP) is an essential stage for slope forming without wall thickness reduction, and the essence of PSRP is the process that the metal in rolling cavity seeking for balanced pressure along axial direction. (2) Unequal slope and unequal wall thickness have obvious effects on stress distribution. (3) We can, through controlling local deformation in PSRP and shortening the time of PSRP, improve the strain and the temperature distribution.

**Keywords** Blank dimension · Conical-section ring · Inco718 alloy · Volume distribution · FE analysis

✉ Dong Liu
liudong@nwpu.edu.cn

Xinglin Zhu
xinglin36@mail.nwpu.edu.cn

Yanhui Yang
yangyh@nwpu.edu.cn

Yang Hu
hy1124@mail.nwpu.edu.cn

Guowei Liu
xianlgw@mail.nwpu.edu.cn

Yuanning Wang
wangyuanning-05@163.com

[1] School of Materials Science and Engineering, Northwestern Polytechnical University, Xi'an 710072, People's Republic of China

[2] TransVIC Technology Co. LTD, Beijing 100102, People's Republic of China

## 1 Introduction

Superalloy rings have been widely used in aerospace engines due to its high temperature performance. With development of manufacturing technology, geometry of engine rings is more and more complex, and the dimensional accuracy is continuously improving. In order to reduce machining allowance and keep integrality of flow lines, profile ring rolling has become a preferred as technique to produce profile rings.

Inco718 alloy possess high deformation resistance and good comprehensive mechanics performance at high temperature. However, the forging temperature range of Inco718 alloy is close limit, while the deformation resistance and microstructure of Inco718 alloy are sensitive to temperature and strain rate. Therefore, in hot ring rolling of Inco718 alloy, the distribution of strain and temperature are both important to the quality of the formed rings.

Different with rectangle ring, the volume distribution of profile ring is changing along axial direction, so it is difficult to control the size evolution and uniformity microstructural of the ring during the ring rolling process. For profile ring rolling, not only process parameter controlling but also reasonable blank design is important to the quality of the formed rings. Some studies have been done regarding profile ring rolling. D. Y. Yang et al. [1–3] researched rolling moment of "L" section ring rolling with energy method. Gunasekera et al. [4, 5] has given a detailed

theoretical analysis on profile ring rolling, which preliminary explored a blank design method of reverse forming. Hawkyard et al. [6, 7] researched the effects of feed speed, friction condition, and groove size to metal flow and section shape of the rings by experimental method. They preliminary explored how to forming ideal section shape when external diameter reached requirement. For a kind of ring with small hole and deep groove, Hua et al. [8] built analytical models of rolling power, torque and force by means of the classic plastic mechanics theory of upper bound method combined with static analysis and calculation of kinematical admissible velocity field. Allwood et al. [9, 10] summarized ring rolling technology and previous researches, including the evolution of rolling equipment design, the methods used to research ring rolling, developments in productive process, and characteristics of all kinds of rings.

With development of finite element method, different finite element models have been explored to research the ring rolling process. Z.M. Hu et al. [11] analyzed process parameters and predicted the defect of fishtail by using an elastic-plastic FEM with a kind of mixed finite element mesh. Also by using similar method, T. Lim et al. [12] saved 70 % time in calculating rectangle ring and L-shape ring rolling process. Song et al. [13] established a coupled thermomechanical 2D FEM of the ring rolling processes of Inco718 alloy. Yea et al. [14] predicted spread, pressure distribution, and roll force during rolling process by using a commercial rigid-plastic FEM. Kim et al. [15] analyzed the rolling process of a profile ring with a round groove located asymmetrically on the outside and found the position of the round groove moves downward and sidewall tilts. Yang et al. [16, 17] researched the effects of the blank sizes and the ratio of axial to radial feed amount during flat ring rolling by 3D FEM. Hua et al. [18–20] presented a controlling method of passive rolls for thick-wall and deep-groove ring rolling and established an online measurement model. Basti et al. [21] analyzed the size effects of forming rolls on strain and temperature distributions by 3D coupled thermomechanical FE simulation. Joun et al. [22] applied a rigid-viscoplastic finite element method to investigate polygonal-shaped defects and developed an improved analysis model with relatively fine finite elements to reduce the computational time. Parvizi et al. [23] validated the present method by using experimental results extracted from ring rolling mill and determined the rolling force when minimizing the upper bound power with respect to neutral point position. Zhou et al. [24] established a mathematic model to predict the ring diameter of the large L-section ring and then verified their result by rigid-plastic finite element (FE) models. Through plenty of work on ring rolling of difficult deformation material, Liu et al. [25, 26] presented a special kind of rolling strategy for rectangular-section ring rolling and found the effects of key parameters on profile ring rolling of superalloy by experimental and FE methods. For double-groove ring, the deforming rules, including diameter growth principle, effect of blank size, and feed velocity, were revealed both by Tian [27] and Li [28] with 3D elastic-plastic finite element method. All these works have revealed the deformation rules effectively and promoted the development of the ring rolling technology.

Through investigation on actual production, profile rings with slope are widely used in aerospace engine such as conical-section ring. A conical-section ring shown in Fig. 1 has the geometrical characteristics of large slope, two straight reach ends and variant diameters of two ends. Due to its geometrical characteristics, in the rolling process of conical-section ring, it is difficult to keep the same diameter and enlarged speed of the two ends; also, the required diameter dimension and cross-section shape are difficult to obtain simultaneously. As shown in Fig. 2, many kinds of defects such as fold, misrun, and edge burr may appear in actual production due to unstable rolling process. Therefore, besides controlling of the rolling process parameters, reasonable blank geometry and dimension are more important to the quality of the conical-section rings.

By comprehensive analysis of existing studies, it can be known that plenty of work has been done to research profile ring rolling. But most of these studies focus on process parameters controlling and industrial analysis with less attention on blank design. So far, there are few studies on forming process of conical-section ring with large slope.

In this paper, an analytical description of the volume distribution characteristic curve (VDCC) is presented. Then, a modified and verified 3D coupled thermomechanical FE model for conical-section ring rolling of Inco718 alloy is established based on FORGE. According to description of VDCC, four blank design principles are presented and their corresponding rolling processes are simulated by the FE model. Finally, dimension effects of the four blanks on forming rules of conical-section ring are analyzed comprehensively.

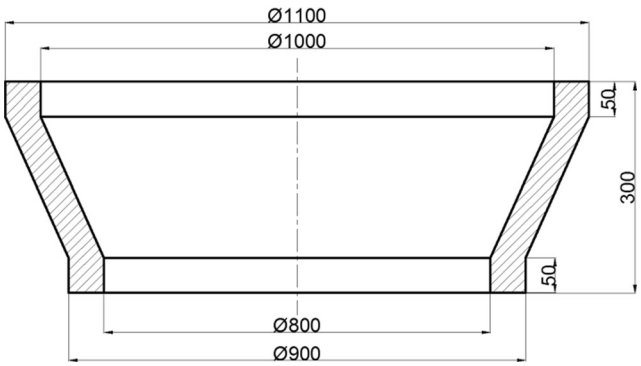


**Fig. 1** Conical-section ring with large slope

(a) Fold (b) Misrun and edge

**Fig. 2** Defects appeared in profile ring rolling. **a** Fold. **b** Misrun and edge

## 2 Description of volume distribution characteristic curve

Axial section of profile ring is nonrectangular, so volume distribution of the ring is changing continuously along axial direction. Because of different volume distribution between blank and ring, metal will flow along both axial and radial directions to fill the rolling cavity.

In order to describe the volume distribution expediently, the VDCC along axial direction is defined as:

$$x = f(y) \tag{1}$$

Axial $y$ is the height direction of the ring. Assuming the ring is parted into $n$ slices, one of whose height is $\Delta y$. We have:

$$n = (y_{\max} - y_{\min})/\Delta y \tag{2}$$

Axial $x$ is the volume radio of one slice to the whole ring. The $y$ of slice $i$ is:

$$y_i = y_{\min} + (i+1)\cdot\Delta y \tag{3}$$

Outside and inside diameters of the axial section have different profile curve as:

$$M = g(y) \tag{4}$$

$$N = z(y) \tag{5}$$

So the volume can be calculated by:

$$V_i = \pi\left(g(y)^2 - z(y)^2\right)\cdot\Delta y \tag{6}$$

$$V = \sum_{1}^{n} \pi\left(g(y)^2 - z(y)^2\right)\cdot\Delta y \tag{7}$$

$$x_i = f(y_i) = V_i/V \tag{8}$$

For a given ring, $f(y_i)$ is an instantaneous variable changing with height. Because the volume variation is continuous, $f(y_i)$ of other height can be obtained by linear interpolation with $f(y_i)$ and $f(y_{i+1})$.

## 3 FE model

### 3.1 Establishment of the FE model

In previous works, FE models for superalloy ring rolling have been analyzed in detail including profile ring [25, 26]. Based on previous works, an improved 3D coupled thermomechanical FE model for conical-section ring rolling of Inco718 alloy is established based on FORGE as shown in Fig. 3. The rolls are established as rigid body and the material of the rolls is 5CrNiMo. The ring is set as deformable body whose material is Inco718. The constitutive model of Inco718 established in previous works [29] is adopted. Penalty function method with penetration restriction and coulombic friction coefficient are used for the contact conditions between ring and rolls. The previous simulation is carried out by using coupled thermomechanical hexahedron elements and the amount of the elements is 8036.

The simulation of conical-section ring rolling requires long calculation time due to the unsteady state of the metal flow. Furthermore, since the size of the ring section continuously changes, the contact conditions between ring and rolls continuously change. In order to improve the accuracy and efficiency of the simulation, three key improvements of the new FE model are proposed and described as follows:

1. According to Arbitrary Lagrangian Eulerian (ALE) approach, a kind of mixed finite element mesh is used

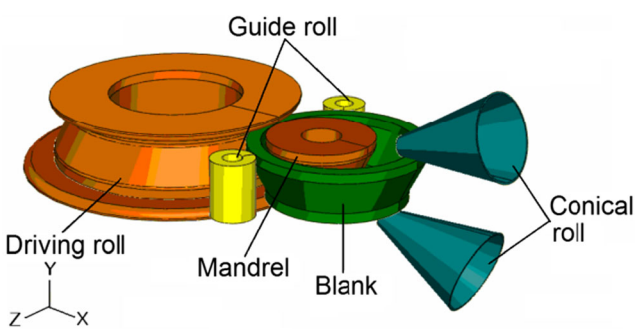


**Fig. 3** FE model of conical-section ring rolling process of Inco718 alloy

in the new FE model as shown in Fig. 4. Different zones of the ring have different mesh sizes. Because the gap zones between kinetic rolls are the main deformation areas of rolling process, so the two parts of the ring are meshed into fine finite elements to improve the calculation accuracy, and the two mesh areas are stationary when the ring rotates. Other parts deviated from the deformation areas have little change of heat, stress, and strain, wherein they are meshed into coarse finite elements to shorten the calculation time. By contrast with the previous model, the new model has better calculation accuracy and about 30 % calculation time reduction in simulation of the conical-section ring rolling.

2. The pressure between the guide rolls and the ring is realized by controlling the force moment of the two guide rolls. The rotation axis is the fixed end of the guide roll arm on rolling equipment, while the length of the force arm is equal to the length of the guide roll arm. By the dynamic controlling of the guide rolls, the new model maintains better consistency with actual production, which can predict all kinds of defects in actual production process such as ellipse and decentration.
3. In this model, two remesh methods can be selected. One is remesh by limiting interval period, and the other one is remesh by limiting deformation. In this study, the prior method is selected to simulate the process of conical-section ring rolling without overlarge deformation. By setting reasonable remesh interval period, calculation time of remesh judging can be saved to improve computational efficiency.

Thermophysical parameters of the two materials and the contact conditions are listed in Table 1, in which the thermal conductivity, Young's modulus, and specific heat are temperature-dependent functions. The motions of the rolls are controlled according to actual production, while the optimal values of the revolving speed of the driving roll and the feeding speed of the mandrel are settled by previous work [26].

**Table 1** Thermophysical parameters

| Parameters | Inco718 | 5CrNiMo |
|---|---|---|
| Density (kg/m$^3$) | 8240 | 7860 |
| Poisson ratio | 0.3 | 0.3 |
| Heat conductivity (W/(m·°C)) | $12.58+0.016\times T$ | 33.5 |
| Young's modulus (GPa) | $208.46–0.094\times T$ | 198 |
| Specific heat (J/(kg·°C)) | $361.21+0.326\times T$ | 448 |
| Temperature (°C) | 1020 | 300 |
| Circumstance temperature (°C) | 20 | |
| Contact heat conductivity (W/(m$^2$·K)) | 900 | |
| Convection coefficient (W/(m$^2$·K)) | 20 | |

### 3.2 Evaluation of the FE model

In order to evaluate the improved FE model, the forming process of a conical-section ring has been simulated by both previous and improved FE models, and then the predicted results are compared with the experimental results.

The experiment was carried out on numerical control ring rolling mill RAW 3000-700 produced by Wagner Banning. Ring material is Inco 718 whose initial temperature is 1020 °C, and the other rolling parameters of the experiment and the simulations stay the same. As shown in Fig. 5, the contour of the formed ring is integrated, while the dimensions meet requirement.

In the experimental ring rolling process, the temperature of the mid height point of outside surface was measured by infrared thermometer and the rolling force along radial direction was obtained by force sensor equipped on the rolling mill. Then, the results of the experiment and the simulations are compared as shown in Fig. 6. It can be seen that the evolution rules of temperature and rolling force of the two models are both coincident with the experiment, while the results of the improved model are more accurate. From the evolution rules of temperature and rolling force simulated by the FE model of this paper, three rolling stages including initial stage, stable rolling stage, and finishing stage can be predicted correctly.

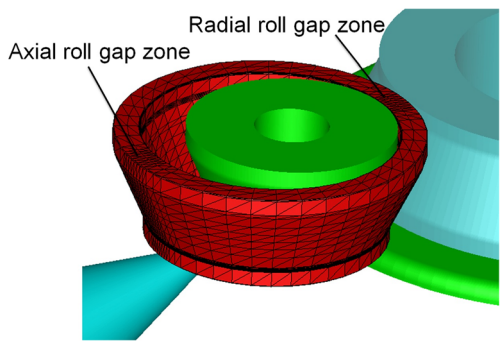


**Fig. 4** Mixed finite element mesh of the ring

**Fig. 5** Formed ring

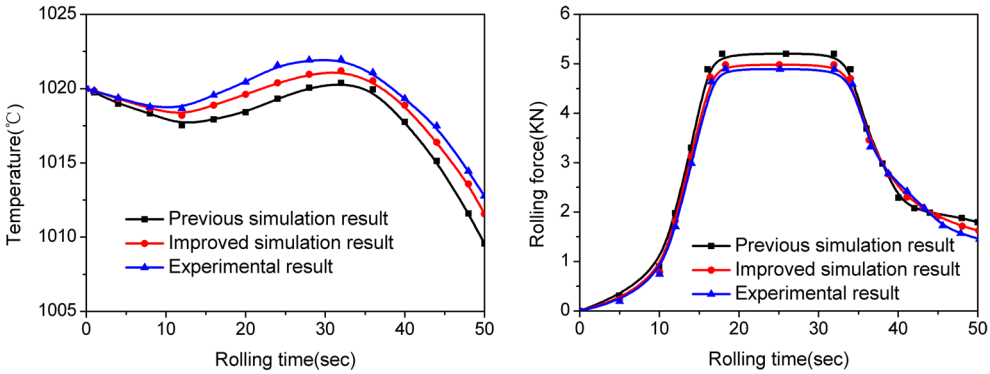


(a) Comparison of temperature (b) Comparison of rolling force

**Fig. 6** Comparison of the simulation results and the experimental results. **a** Comparison of temperature. **b** Comparison of rolling force

The error value of the simulated temperature is less than 3 °C, while the error range of the simulated rolling force is less than 5 %. All above analysis verifies the reliability of the improved FE model established in the paper, which can be used to research the profile ring rolling process adequately.

## 4 Blank dimension description

Based on description of volume distribution characteristic curve (VDCC) and the reliable FE model, four blank design principles are presented. Then, dimension effects of conical-section blanks on dimensional accuracy and thermomechanical parameters distribution are analyzed.

The dimensions of a conical-section blank can be described by the mean diameters $D_{L0}$, $D_{S0}$, the thickness $h_{L0}$, $h_{S0}$, the axial height $b_0$, $b_{L0}$, $b_{S0}$ and the slope $\theta_{a0}$, $\theta_{b0}$, as illustrated in Fig. 7. Based on principle of volume invariably, three constraint conditions are presented as blank design basis: (1) equal volume distribution along axial direction, (2) equal slope of mean line, and (3) equal thickness of the two ends.

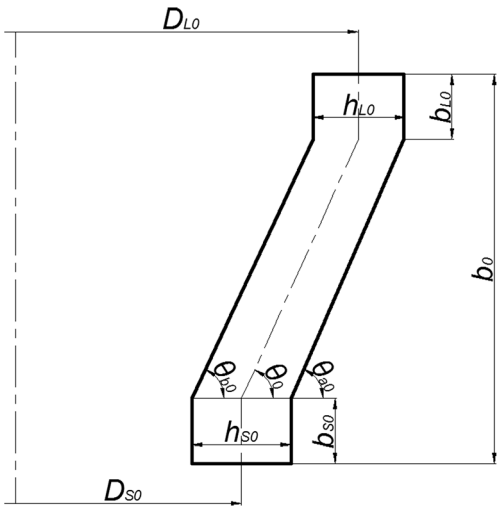


**Fig. 7** Description of conical-section blank dimensions

According to above basis, four blank design principles are presented as follows:

1. Rectangular ring blank is easier to be produced than profile ring blank. Conical-section ring rolling with rectangular ring blank is simulated firstly in this article. Thickness of rectangular ring blank is settled by the thickness ratio of the small end (Eq. (9)). Rectangular ring blank just follows Constraint 3.

$$k = h_0/h \tag{9}$$

Then, according to the principle of volume invariably, mean diameter of the blank $D_{L0}$ ($D_{S0}$) is settled. Comparisons of sectional dimension and volume distribution along axial direction between blank 1 and formed ring are shown in Fig. 8a, e.

2. The thicknesses of two ends ($h_{L0}$,$h_{S0}$) are settled firstly by Eq. (9). Then, according to Constraint 1, mean diameters of two ends ($D_{L0}$,$D_{S0}$) are settled. Constraint 2 is free. Comparisons of sectional dimension and volume distribution along axial direction between blank 2 and formed ring are shown in Fig. 8b, f. The two volume distribution curves overlap due to Constraint 1.
3. Thickness and mean diameter of the large end ($h_{L0}$,$D_{L0}$) are settled in turns by Eq. (9) and Constraint 1. Then, according to Constraint 2, slope of mean line is settled, $\theta_0=\theta$. Mean diameter and thickness of the small end ($D_{S0}$, $h_{S0}$) are settled in turns by Eq. (10) and Constraint 1. Constraint 3 is free. Comparisons of sectional dimension and volume distribution along axial direction between blank 3 and formed ring are shown in Fig. 8c, g.

$$D_{S0} = D_{L0} - 2(b_0 - b_{L0} - b_{S0})\cdot \cot\theta_0 \tag{10}$$

4. The thickness of two ends ($h_{L0}$,$h_{S0}$) and slope of mean line are settled by Eq. (9) and Constraint 2. Then, according to the principle of volume invariably and Eq. (10), mean diameters of two ends ($D_{L0}$,$D_{S0}$) are settled, as

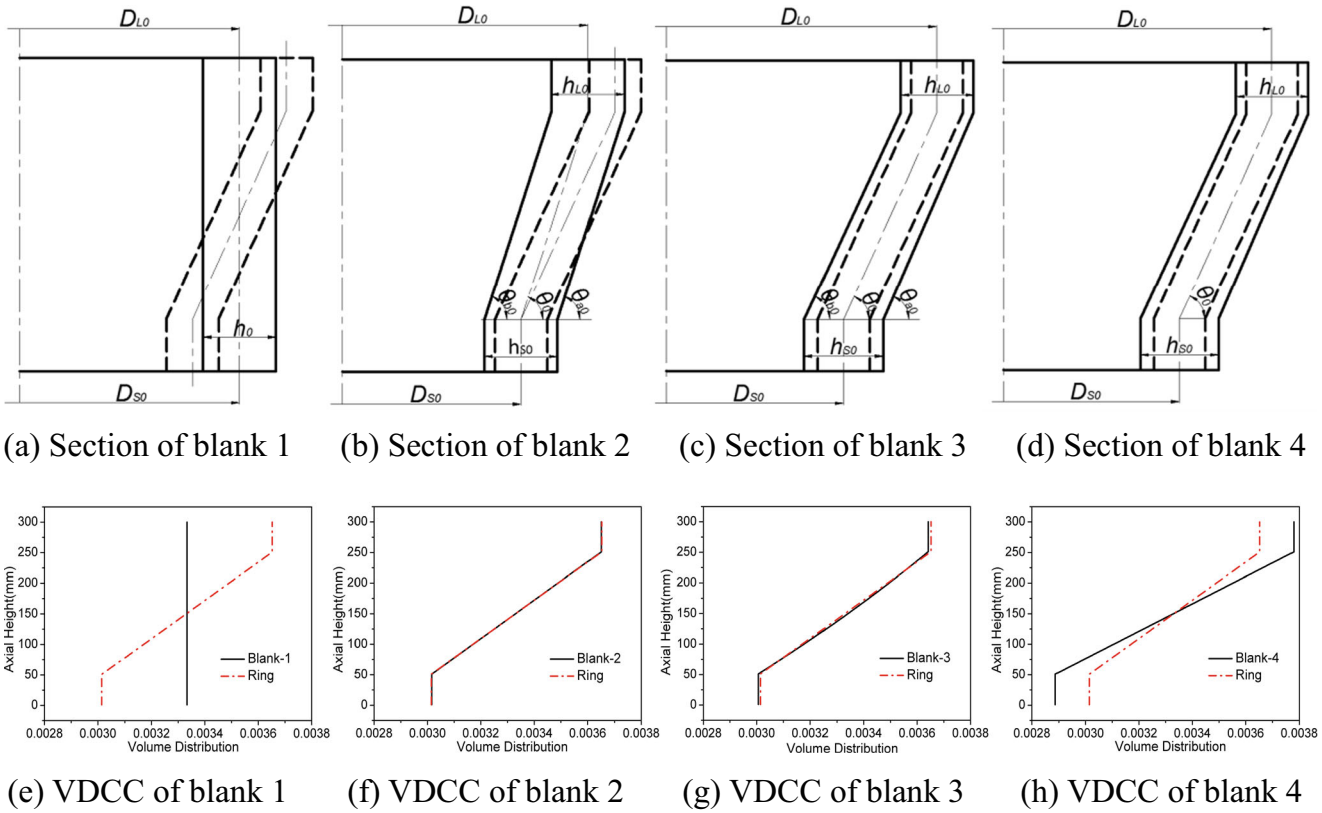


**Fig. 8** Comparisons between blanks and formed ring. **a** Section of blank 1. **b** Section of blank 2. **c** Section of blank 3. **d** Section of blank 4. **e** VDCC of blank 1. **f** VDCC of blank 2. **g** VDCC of blank 3. **h** VDCC of blank 4

illustrated by Eqs. (11), (12), and (13). Comparisons of sectional dimension and volume distribution along axial direction between blank 4 and formed ring are shown in Fig. 8d, h. Constraint 1 is free.

$$V_{\text{Ring}} = V_{\text{Blank}} = f(D_{L0}, h_{L0}, D_{S0}, h_{S0}) \tag{11}$$

$$D_{S0} = g(D_{L0}, \theta_0) \tag{12}$$

$$V_{\text{Blank}} = F(D_{L0}) \tag{13}$$

Four blanks are designed to contain all dimension factors. Blanks 2, 3, and 4 are conical-section blanks and each of them ignores one constraint. Dimension effects of blanks for conical-section ring rolling can be analyzed comprehensively by the four blanks.

## 5 Result and discussion

### 5.1 Evolution of the ring dimension

Conical-section ring rolling is an integrated process of wall reduction, diameter evolution, and slope forming. Dimensional

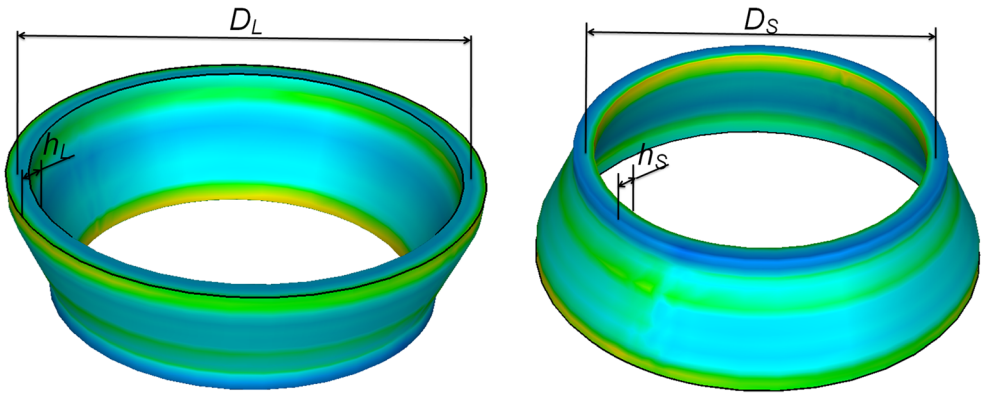


**Fig. 9** Formed ring

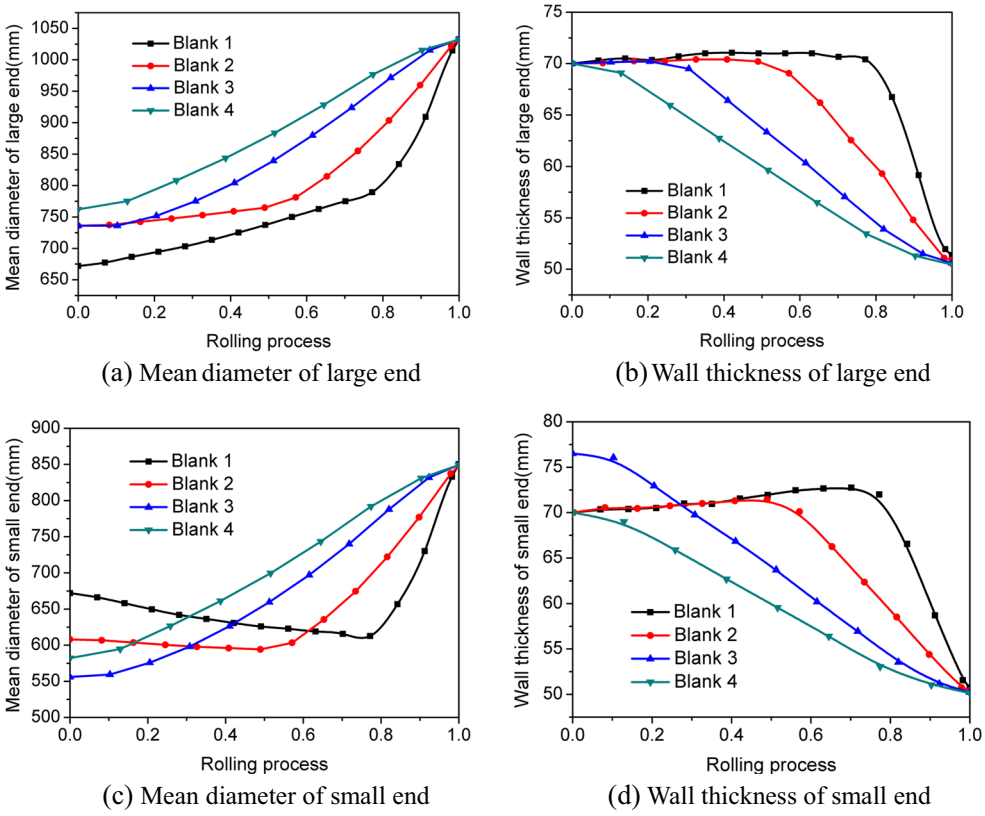


(a) Mean diameter of large end (b) Wall thickness of large end

(c) Mean diameter of small end (d) Wall thickness of small end

**Fig. 10** Dimension evolution with rolling process. **a** Mean diameter of large end. **b** Wall thickness of large end. **c** Mean diameter of small end. **d** Wall thickness of small end

accuracy and uniformity of the strain and temperature distribution are secured by coordination control of every dimension. By simulation with above models, a formed ring is shown in Fig. 9.

The geometric dimensions of four formed rings are measured and compared. Evolution curves of $D_L$, $D_S$, $h_L$, and $h_S$ of the four blanks are shown in Fig. 10, respectively. As shown in Fig. 10a, $D_L$ of blanks 1 and 2 grow up slowly before 80 and 60 % of their respective rolling process, while the $h_L$ remains unchanged in principle (Fig. 10b). We can define this rolling stage as preparation stage of rolling process (PSRP). Also in Fig. 10c, d, $D_S$ decrease gradually and $h_S$ has little change during PSRP. Since there is little change of the wall thickness, we can deduce that the rolling preparation stage is just stage for slope forming without wall thickness reduction. Diameter

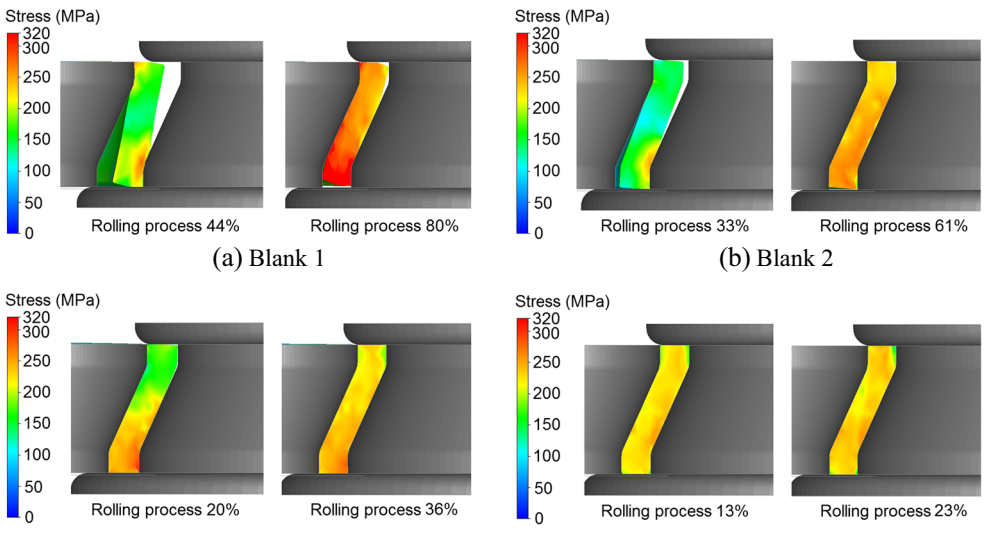


(a) Blank 1 (b) Blank 2

(a) Blank 3 (b) Blank 4

**Fig. 11** Stress distribution of axial section at different rolling process

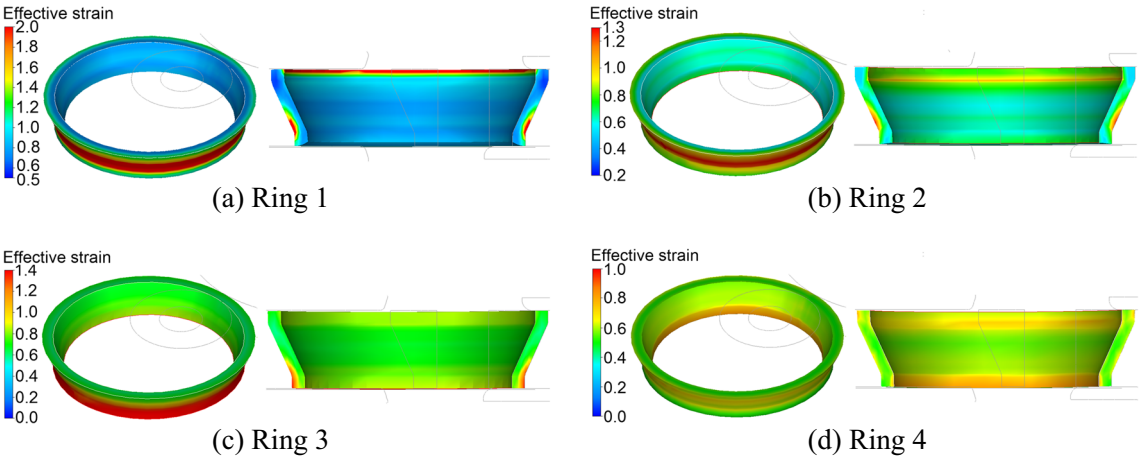


**Fig. 12** Effective strain distribution of formed ring

growth of the ring mainly takes place in the stage after PSRP relying on metal's radial deformation. Because of unequal slope with formed ring, blanks 1 and 2 have a long PSRP, while blanks 3 and 4 have a short PSRP due to equal slope.

### 5.2 Stress distribution and evolution

Figure 11 illustrates stress distribution at different rolling process of the four blanks. It can be seen in PSRP of blanks 1 and 2, driving roll and mandrel are contact with small end and large end of the blank, respectively. Torque is generated on the axial section due to unbalanced pressure along both axial and radial direction produced by rolls. At PSRP of blank 3, larger pressure is generated at the small end because rolls contact firstly at the thicker end. The maximum stress zones of blanks appear at outside of the small end where contact firstly with driving roll. Because of equal slope and equal wall thickness with formed ring along axial direction, blank 4 has uniform stress at the early stage of the rolling.

After PSRP, stress distribution tends to uniform, when the wall thickness begins to reduce and the diameters begin to grow up (Fig. 11). We can deduce that the essence of PSRP is the process that the metal in rolling cavity seeking for balanced pressure along axial direction. PSRP of blank 1 occupy 80 % of the whole rolling process, which lead to the deformation zone with non-uniform stress distribution for a long time. In actual production, radial dimensions are formed mainly in the last stage of the rolling. For this kind of forming process, unbalanced pressure and unreasonable deformation process lead to unstable dimensional accuracy, filling defect, and non-uniform microscopic structure.

### 5.3 Strain distribution and evolution

Figure 12 shows effect plastic strain distribution of four formed rings. It can be seen that ring 4 has the best uniformity of strain distribution, while ring 1 has the worst uniformity. Due to unequal slope, the maximum strain of blank 1 and 2 appear at the corner of the small end where contact with the driving roll. Also due to larger wall thickness, the maximum strain of blank 3 appears at outside of the small end. The maximum strain zones are just the maximum stress zones in their respective PSRP. Eleven trace points A–K (as shown in Fig. 13) are selected to investigate the strain variation and distribution during the rolling process.

Effective strains of points A–K during the rolling process are picked to make into curves, as shown in Fig. 14. It can be seen from Fig. 14a, b that their PSRP can be divided into two parts. In the first part, local deformation appears at the contact areas between the ring and the rolls (points A, C, I and K). In the second part, concentrated stress begin to spread along the axial section and stress distribution tend to uniform, so local deformation did not appear in the second part of PSRP. After PSRP, strains of all trace points increase rapidly due to metal's flow along circumferential and radial directions. Figure 14c shows that before 40 % of the rolling process, strain of points A and C contacted with the driving roll increases rapidly due to the thicker wall. After 40 %, all points have nearly the same strain rate. All points of ring 4 (Fig. 14d) have the most similar strain variation curves.

The grain of the metal can be refined in the area of large strain, but forming damage also more likely occurs in this area.

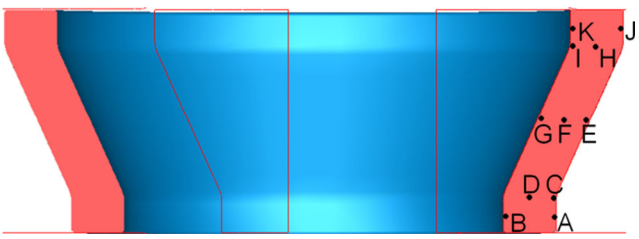


**Fig. 13** Location of trace points

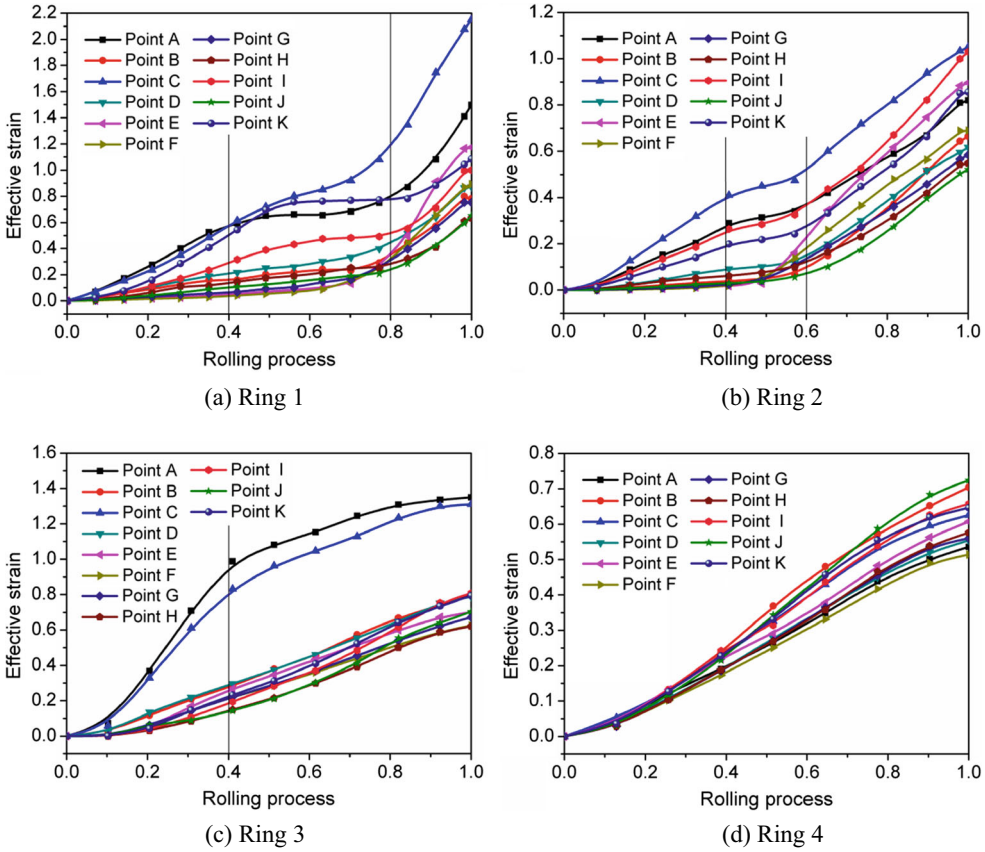


**Fig. 14** Variation of effective strain

The extreme values and fluctuating range of strain are important to grain size and microstructure heterogeneity. The index for the uniformity of the effective strain distribution is defined as:

$$S_\varepsilon = \sqrt{\frac{1}{n}\sum_{i=1}^{n}(\varepsilon_i - \bar{\varepsilon})^2} \tag{14}$$

where $\varepsilon_i$ is the effective strain value of the trace point, and $\bar{\varepsilon}$ is the average effective strain of trace points. The lesser the $S_\varepsilon$, the more uniform the strain distribution, while the microstructure becoming more uniform. As shown in Table 2, blank 1 has the maximum fluctuating range and maximum $S_\varepsilon$, which is certain to lead to large residual stress and uneven microstructure, so forming conical-section ring with rectangle blank is improper. From the data of blanks 2 and 3, we can see that the effects of slope and wall thickness are obvious on strain fluctuation and uniformity. From the data of blank 4, we can see that unequal volume distribution along axial direction within certain limits is little effect on strain uniformity. Therefore, we can, through controlling local deformation in PSRP, improve strain distribution. Advantage of the strain distribution can be summarized as ring 4>ring 2>ring 3>ring 1.

**Table 2** Effective strain date of the four rings

| | $\varepsilon_{max}$ | $\varepsilon_{min}$ | Range | $\bar{\varepsilon}$ | $S_\varepsilon$ |
|---|---|---|---|---|---|
| Blank 1 | 2.150 | 0.634 | 1.516 | 1.045 | 0.445 |
| Blank 2 | 1.050 | 0.522 | 0.528 | 0.753 | 0.188 |
| Blank 3 | 1.350 | 0.640 | 0.710 | 0.835 | 0.254 |
| Blank 4 | 0.724 | 0.514 | 0.210 | 0.609 | 0.069 |

### 5.4 Temperature distribution and evolution

Figure 15 shows temperature distribution of four formed rings. It can be seen that ring 4 has the best uniformity of temperature. Due to longer rolling time, low temperature zones of blanks 1 and 2 appear at the two ends along axial direction. Also due to larger wall thickness, the higher temperature of blank 3 appears at center part of the small end. Eleven trace points A–K (as shown in Fig. 13) are selected to investigate the temperature variation and distribution during the rolling process.

Temperatures of points A–K during the rolling process are picked to make into curves, as shown in Fig. 16. It can be seen from Fig. 16a, b that in their PSRP, temperatures of all points decrease gradually, especially the points close to surface. Exceptionally, temperature decrease velocity of point C is lower than that in other points, which is because the local deformation that appeared here has produced deformation heat. After PSRP, temperatures of all trace points

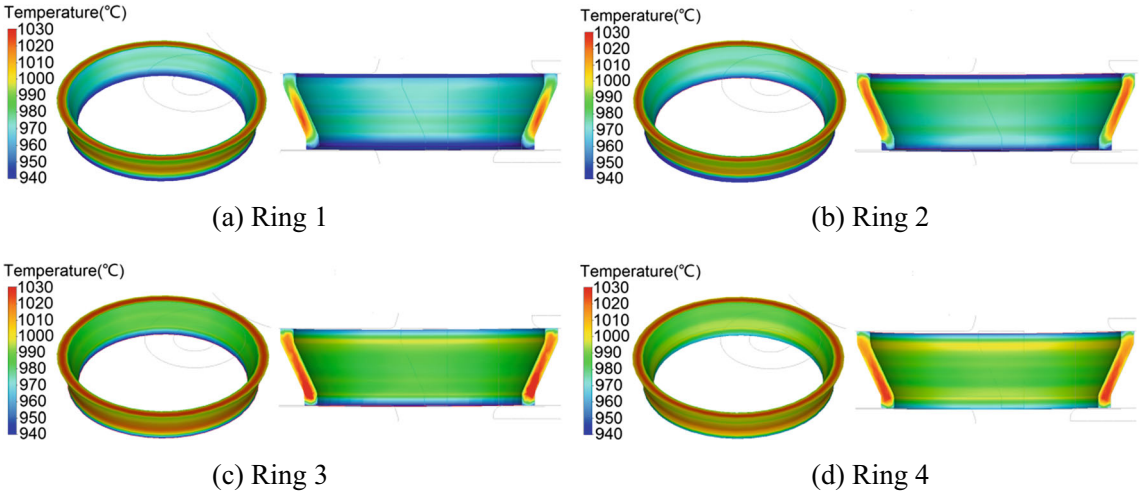


**Fig. 15** Temperature distribution of formed ring

increase rapidly due to global deformation of the metal in rolling cavity. Figure 16c shows that temperatures of center points (D, F, H) and point C are not decreased in the whole rolling process, which is because of shorter PSRP and earlier global deformation. All points of ring 4 (Fig. 16d) have no great temperature changes due to more uniform global deformation.

The temperature drop may result in the reduction of metal's plasticity and static recrystallization, which is harmful for the forming process. The extreme values and fluctuating range of temperature are important to grain size and microstructure heterogeneity. The index for the uniformity of the temperature distribution is defined as:

$$S_T = \sqrt{\frac{1}{n}\sum_{i=1}^{n}(T_i - \bar{T})^2} \tag{15}$$

**Fig. 16** Variation of temperature

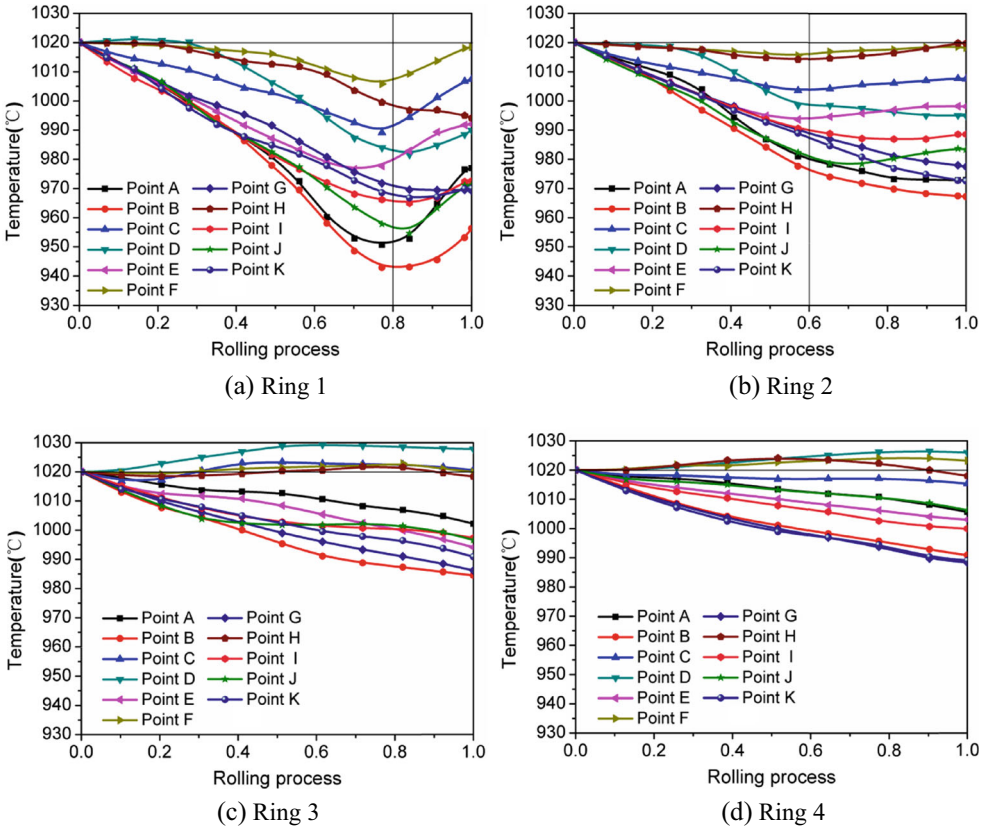

**Table 3** Temperature date of the four rings

| | $T_{max}$ (°C) | $T_{min}$ (°C) | Range (°C) | $\overline{T}$ (°C) | $S_T$ (°C) |
|---|---|---|---|---|---|
| Blank 1 | 1018.5 | 956.2 | 62.3 | 983.4 | 18.6 |
| Blank 2 | 1019.8 | 967.3 | 52.5 | 991.0 | 18.4 |
| Blank 3 | 1027.8 | 984.5 | 43.3 | 1003.5 | 15.4 |
| Blank 4 | 1026 | 988.3 | 37.7 | 1005.9 | 13.4 |

where $T_i$ is temperature value of the trace point, and $\overline{T}$ is average temperature of trace points. The lesser the $S_T$, the more uniform the temperature, while the microstructure becoming more uniform. As shown in Table 3, blanks 1 and 2 have lower $T_{min}$, larger fluctuating range, and bigger $S_T$, that is because long PSRP result in more heat loss. From the data of blank 3, we can see that the effect of wall thickness on temperature is little due to the counteraction between deformation heat and heat loss. From the data of blank 4, we can see that unequal volume distribution along axial direction within certain limits has little effect on temperature distribution. Therefore, we can, through shortening the time of PSRP, improve temperature distribution. Advantage of the temperature distribution can be summarized as ring 4>ring 3>ring 2>ring 1.

## 6 Conclusions

For conical-section ring rolling of Inco718, four blank design principles are presented based on analytical description of the VDCC, and the dimension effects of blanks on dimensional accuracy and thermomechanical parameters distribution are explored by using a reliable 3D coupled thermomechanical FE model. The conclusions can be summarized as:

1. PSRP is an essential stage for slope forming without wall thickness reduction. Diameter growth of the ring mainly takes place in the stage after PSRP relying on metal's radial deformation.
2. Unequal slope and unequal wall thickness have obvious effects on stress distribution. The essence of PSRP is the process that the metal in rolling cavity seeking for balanced pressure along axial direction.
3. We can, through controlling local deformation in PSRP and shortening the time of PSRP, improve the strain and the temperature distribution
4. According to the effects of all dimension factors analyzed above, design principle of blank 4 is most suitable for conical-section ring rolling.

**Acknowledgments** The authors would like to thank the Specialized Research Fund for the Doctoral Program of Higher education (No.20126102120022) and Northwestern Polytechnical University (NPU) Foundation for Fundamental Research (NPU-FFR-JC200822) for the support given to the research.

## References

1. Yang DY, Ryoo JS, Chol JC, Johnson W (1981) Analysis of roll torque in profile ring-rolling of L-section. Proc 21st Int MTDR Conf, London, pp 69–74
2. Ryoo JS, Yang DY, Johnson W (1983) Ring rolling: the inclusion of pressure roll speed for estimating torque by using a velocity supper position method. Proc 24th Int MTDR Conf, Manchester, pp 19–24
3. Yang DY, Ryoo JS (1987) An investigation into the relationship between torque and load in ring rolling. J Eng Ind ASME Trans 109(8):190–196
4. Gunasekera J, Jia Z, Malas J (1998) Analysis of aluminum extrusion processes using upper bound element technique. Processing Third World Conference On Integrated Design and Process Technology, Berlin, pp 215–220
5. Ranatunga PV, Gunasekera J, Hur K (2001) Use of UBET for design of flash gap in closed die forging. J Mater Process Technol 111:107–112
6. Hawkyard JB, Ingham PM (1979) An investigation into profile ring rolling. Proc 1st Int Conf on ROMP, London 20:64–66
7. Hawkyard JB, Moussa G (1984) Studies of profile development and roll force in profile ring Rolling. Proc 3rd Int Conf on ROMP, Kyoto 10:267–278
8. Hua L, Deng JD, Qian DS, Ma Q (2015) Using upper bound solution to analyze force parameters of three-roll cross rolling of rings with small hole and deep groove. Int J Adv Manuf Technol 76:353–366
9. Allwood JM, Tekkaya AE, Stanistreet TF (2005) The development of ring rolling technology. Steel Res Int 76(2/3):111–120
10. Allwood JM, Tekkaya AE, Stanistreet TF (2005) The development of ring rolling technology. Part2. Investigation of process behavior and production equipment. Steel Res Int 76(7):491–507
11. Hu ZM, Pillinger I, Hartley P, McKenzie S, Spence PJ (1994) Three-dimensional finite-element modelling of ring rolling. J Mater Process Technol 45:143–148
12. Lim T, Pillinger I, Hartley P (1998) A finite-element simulation of profile ring rolling using a hybrid mesh model. J Mater Process Technol 80–81:199–205
13. Song JL, Dowson AL, Jacobs MH, Brooks J, Beden I (2002) Coupled thermo-mechanical finite-element modeling of hot ring rolling process. J Mater Process Technol 121(2/3):332–340
14. Yea YS, Ko YS, Kim NS, Lee JC (2003) Pressure distribution and roll force in ring rolling process using rigid-plastic finite element method. J Mater Process Technol 140(1/3):478–486
15. Kim KH, Suk HG, Huh MY (2007) Development of the profile ring rolling process for large slewing rings of alloy steels. J Mater Process Technol 187–188:730–733
16. Yang H, Wang M, Guo LG, Sun ZC (2008) 3D coupled thermo-mechanical FE modeling of blank size effects on the uniformity of strain and temperature distribution during hot rolling of titanium alloy large rings. Comput Mater Sci 44:611–621
17. Zhu S, Yang H, Guo LG, Hu LL, Chen XQ (2014) Research on the effects of coordinate deformation on radial-axial ring rolling process by FE simulation based on in-process control. Int J Adv Manuf Technol 72:57–68
18. Qian DS, Zhang ZQ, Hua L (2013) An advanced manufacturing method for thick-wall and deep-groove ring-combined ring rolling. J Mater Process Technol 213:1258–1267

19. Wang XK, Hua L, Han XH, Wang XX, Wang DH, Liu YL (2014) Numerical simulation and experimental study on geometry variations and process control method of vertical hot ring rolling. Int J Adv Manuf Technol 73:389–398
20. Wang XK, Hua L (2013) Modeling of on-line measurement for rolling the rings with blank size errors in vertical hot ring rolling process. Int J Adv Manuf Technol 68:257–262
21. Anjami N, Basti A (2010) Investigation of rolls size effects on hot ring rolling process by coupled thermo-mechanical 3D-FEA. J Mater Process Technol 210:1364–1377
22. Moon HK, Lee MC, Joun MS (2008) Predicting polygonal-shaped defects during hot ring rolling using a rigid-viscoplastic finite element method. Int J Mech Sci 50:306–314
23. Parvizi A, Abrinia K (2014) A two dimensional upper bound analysis of the ring rolling process with experimental and FEM verifications. Int J Mech Sci 79:176–181
24. Zhou PZ, Zhang LW, Gu SD, Ruan JH, Teng LH (2014) Mathematic modeling and FE simulation of radial-axial ring rolling large L-section ring by shape axial roll. Int J Adv Manuf Technol 72:729–738
25. Liu D, Fu MJ, Wan ZY, Yang Y, Zhang H (2007) Rolling strategies in the rolling process of GH4169 alloy with rectangle cross-section ring. Acta Aeronaut Astronaut Sin 28(5):1276–1280 **(in Chinese)**
26. Ma YW, Wang ZH, Liu D, Zhu XL, Yang ZS (2011) Optimization of rotational speed of driving roll in profile ring rolling of GH4169 alloy. Acta Aeronaut Astronaut Sin 32(8):1276-1280&1555-1562 (in Chinese)
27. Tian L, Luo Y, Mao HJ, Hua L (2013) A hybrid of theory and numerical simulation research for virtual rolling of double-groove ball rings. Int J Adv Manuf Technol 69:1–13
28. Li LY, Li X, Liu J, He Z (2013) Modeling and simulation of cold rolling process for double groove ball-secti on ring. Int J Adv Manuf Technol 69:1717–1729
29. Liu D, Luo ZJ (2005) Method for establishment of constitutive relationship based on microstructural evolution. J Plast Eng 12: 54–57 **(in Chinese)**